Supplementary Information for

Theoretical and experimental investigation on the intersystem crossing kinetics in benzothioxanthene imide luminophores, and their dependence on substituents effects.

Laura Abad Galán,[a] José M. Andrés Castán,[b] Clément Dalinot,[b] Pablo Simón Marqués,[b] Philippe Blanchard,[b] Olivier Maury,[a] Clément Cabanetos,[b*] Tangui Le Bahers,[a*] Cyrille Monnereau[a*]

[a.] *Univ. Lyon, ENS Lyon, CNRS, Université Lyon 1, Laboratoire de Chimie, UMR 5182, 46 Allée d'Italie, 69364 Lyon, France*
[b.] *Group Linear Conjugated Systems, MOLTECH-Anjou, CNRS UMR 6200, University of Angers, Angers, France.*

Scheme S1. General procedure for the synthesis of the BTXI-SO2 derivatives.

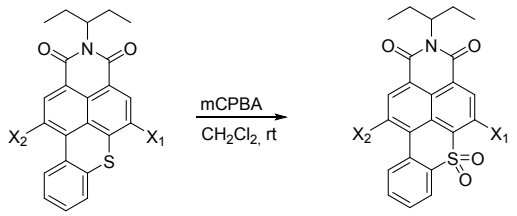

BTXI-SO_2 (X_1=H, X_2=H) = 100%
BTXI-SO_2-Br (X_1=Br, X_2=H) = 74%
BTXI-SO_2-NO_2 (X_1=NO_2, X_2=H) = 74%
BTXI-SO_2-I (X_1=I, X_2=H) = 31%
BTXI-SO_2-BrBr (X_1=Br, X_2=Br) = 19%

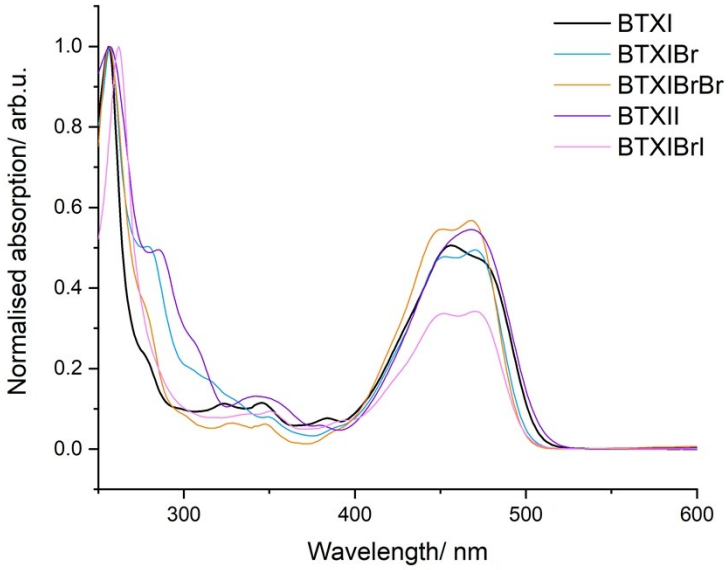

Figure S1. - Normalised absorbance of the BTXI derivatives in DCM at room temperature.

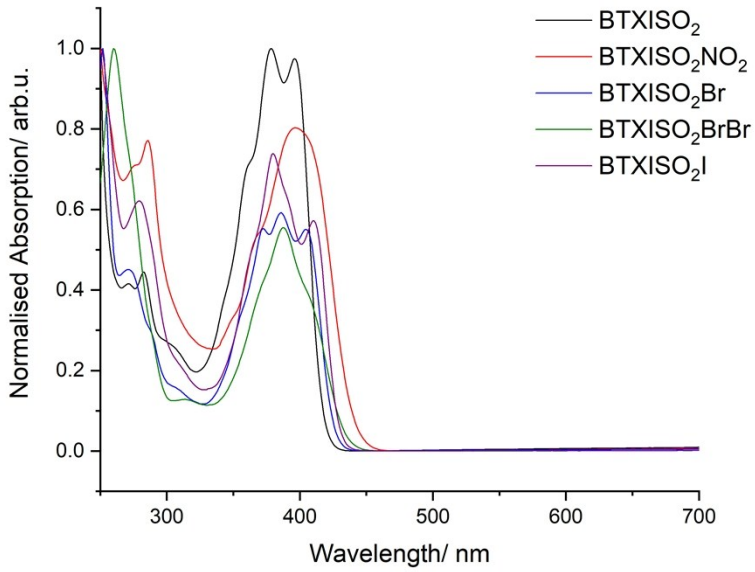

Figure S2. Normalised absorption of the BTXI-SO_2 derivatives in DCM at room temperature.

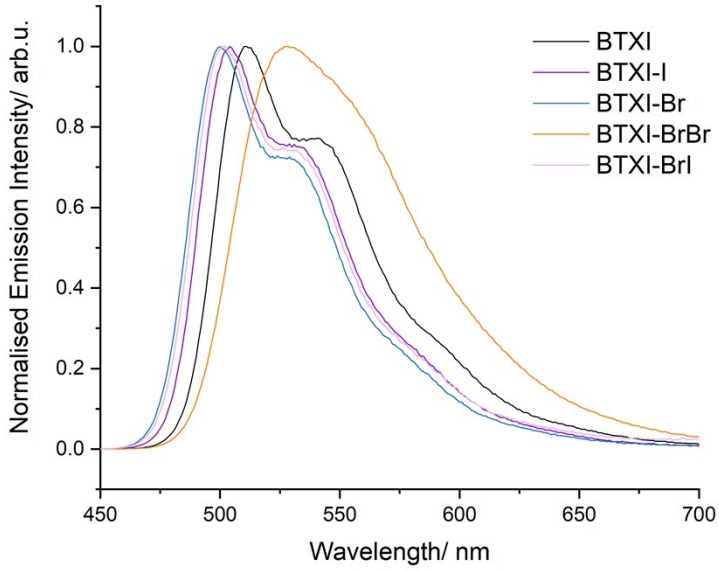

Figure S3. Normalised emission (λ_{exc}= 425 nm) of the BTXI derivatives in DCM at room temperature.

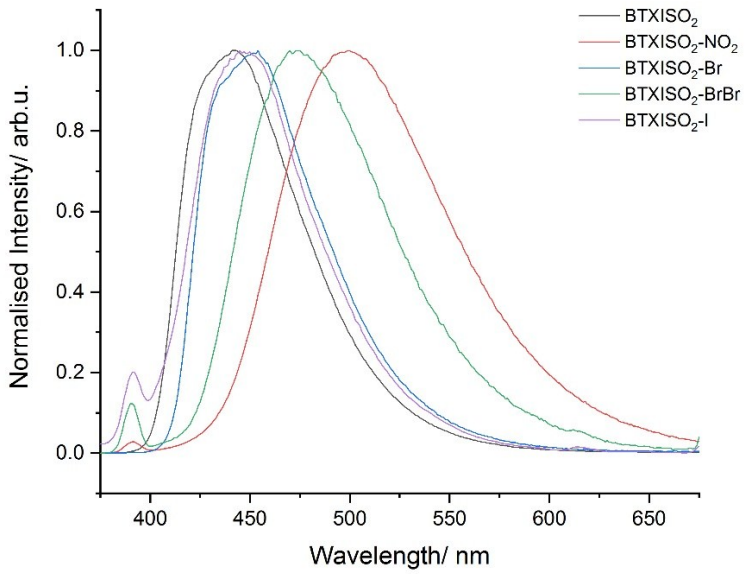

Figure S4. Normalised emission (λ_{exc}= 375 nm) of the BTXI-SO_2 derivatives in DCM at room temperature.

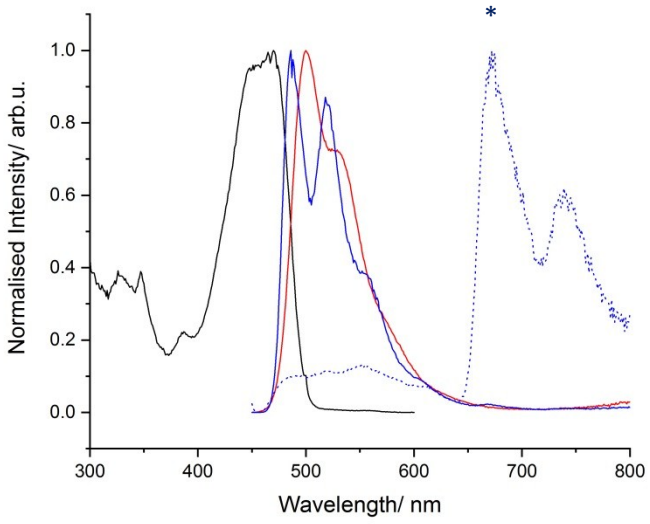

Figure S.5. Normalised excitation (λ_{em}= 585 nm) (black trace), emission (λ_{exc}= 425 nm) at room temperature (red trace) and at 77K in a mixture MeOH:EtOH (1:4) without (blue solid trace) and with a 0.05 ms delay (blue dotted trace) of BTXI-Br.

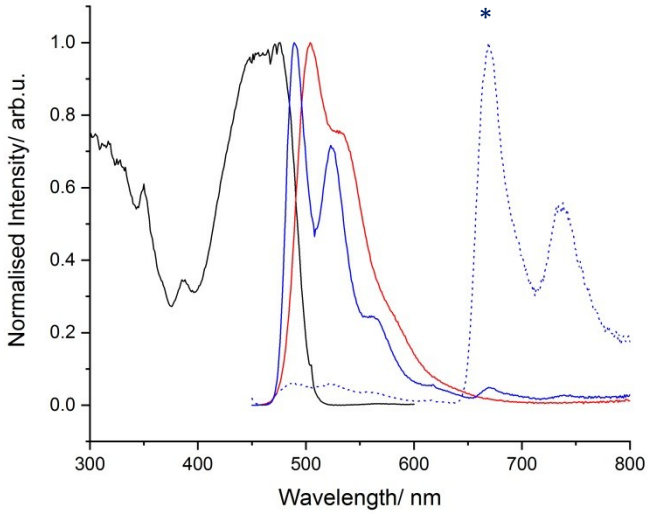

Figure S.6. Normalised excitation (λ_{em}= 585 nm) (black trace), emission (λ_{exc}= 425 nm) at room temperature (red trace) and at 77K in a mixture MeOH:EtOH (1:4) without (blue solid trace) and with a 0.05 ms delay (blue dotted trace) of BTXI-I.

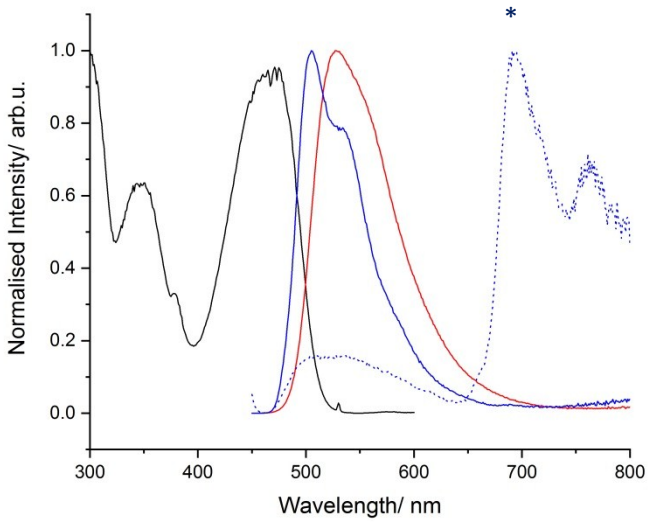

Figure S.7. Normalised excitation (λ_{em}= 585 nm) (black trace), emission (λ_{exc}= 425 nm) at room temperature (red trace) and at 77K in a mixture MeOH:EtOH (1:4) without (blue solid trace) and with a 0.05 ms delay (blue dotted trace) of BTXI-BrBr.

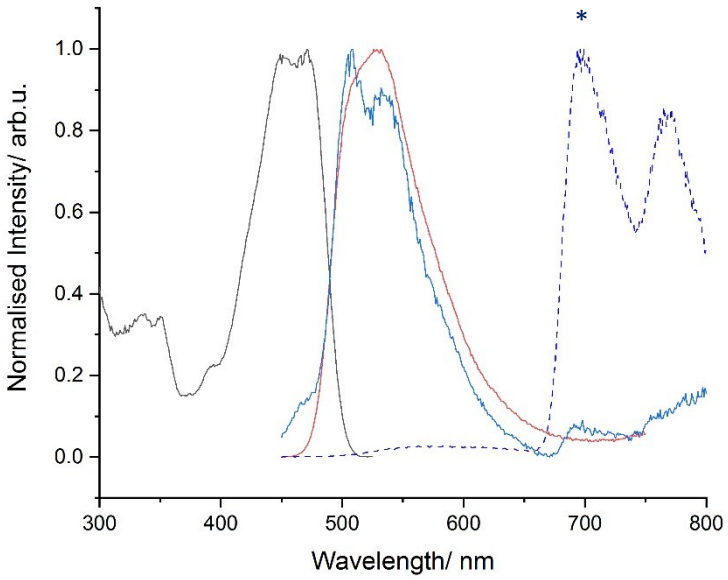

Figure S.8. Normalised excitation (λ_{em}= 550 nm) (black trace), emission (λ_{exc}= 425 nm) at room temperature (red trace) and at 77K in a mixture MeOH:EtOH (1:4) without (blue solid trace) and with a 0.05 ms delay (blue dotted trace) of BTXI-BrI.

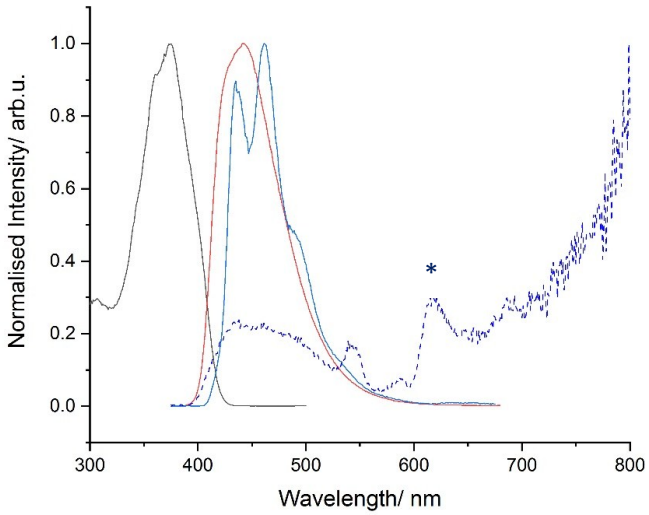

Figure S.9. Normalised excitation (λ_{em}= 442 nm) (black trace), emission (λ_{exc}= 375 nm) at room temperature (red trace) and 77K in a mixture MeOH:EtOH (1:4) (blue trace) of BTXI-SO_2.

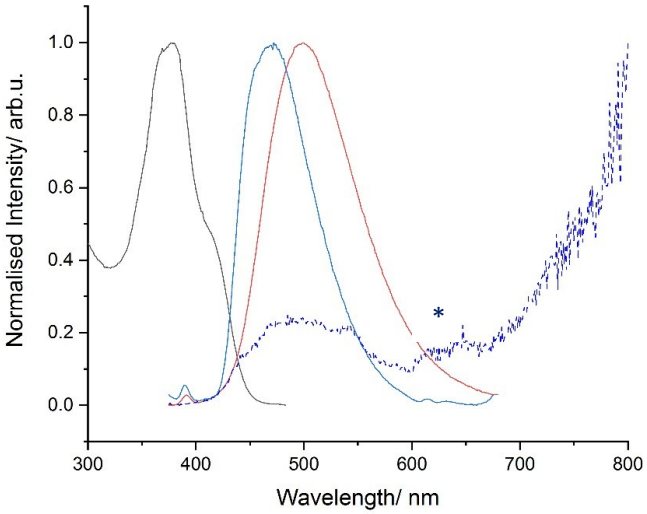

Figure S.10. Normalised excitation (λ_{em}= 495 nm) (black trace), emission (λ_{exc}= 375 nm) at room temperature (red trace) and 77K in a mixture MeOH:EtOH (1:4) (blue trace) of BTXI-SO_2-NO_2.

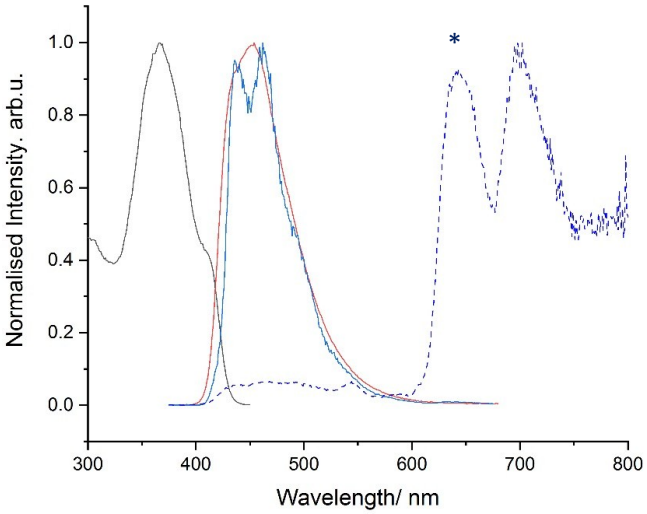

Figure S.11. Normalised excitation (λ_{em}= 455 nm) (black trace), emission (λ_{exc}= 375 nm) at room temperature (red trace) and 77K in a mixture MeOH:EtOH (1:4) (blue trace) of BTXI-SO_2-Br.

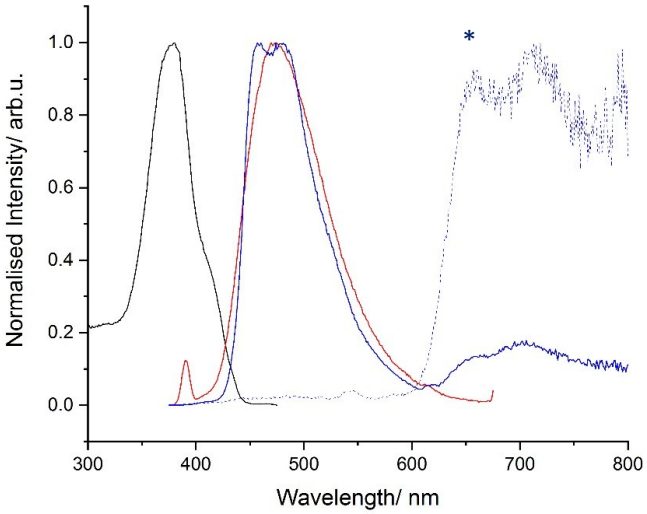

Figure S.12.- Normalised excitation (λ_{em}= 500 nm) (black trace), emission (λ_{exc}= 375 nm) at room temperature (red trace) and 77K in a mixture MeOH:EtOH (1:4) (blue trace) of BTXI-SO_2-BrBr.

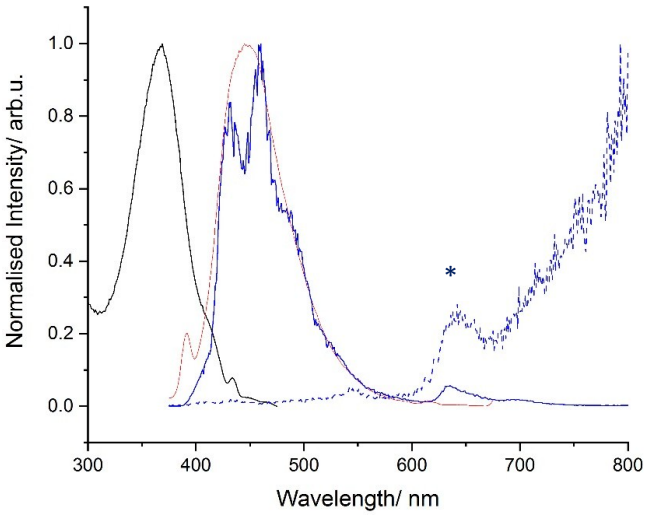

Figure S.13.- Normalised excitation (λ_{em}= 500 nm) (black trace), emission (λ_{exc}= 375 nm) at room temperature (red trace) and 77K in a mixture MeOH:EtOH (1:4) (blue trace) of BTXI-SO_2-I.

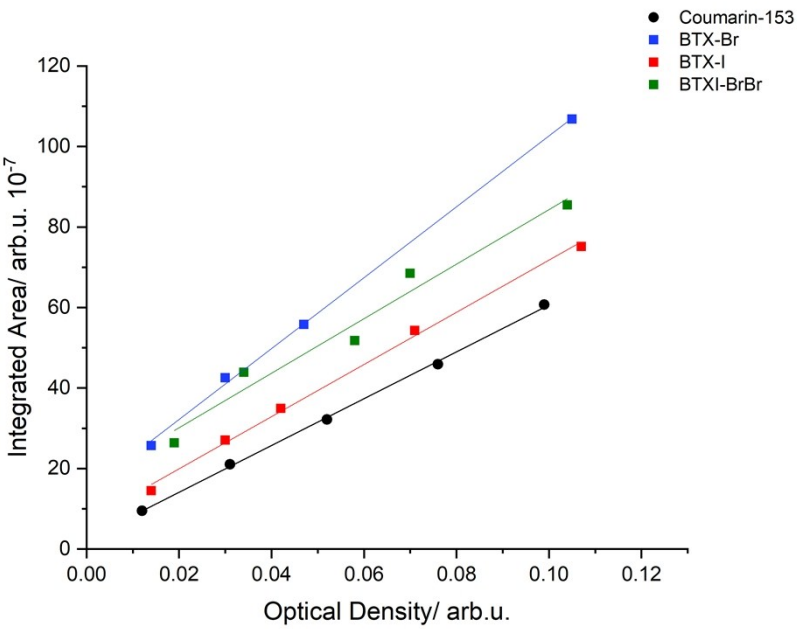

Figure S.14.- Integrated emission area according to optical density of Coumarine-153 (black line) and the BTXI derivatives in DCM at room temperature.

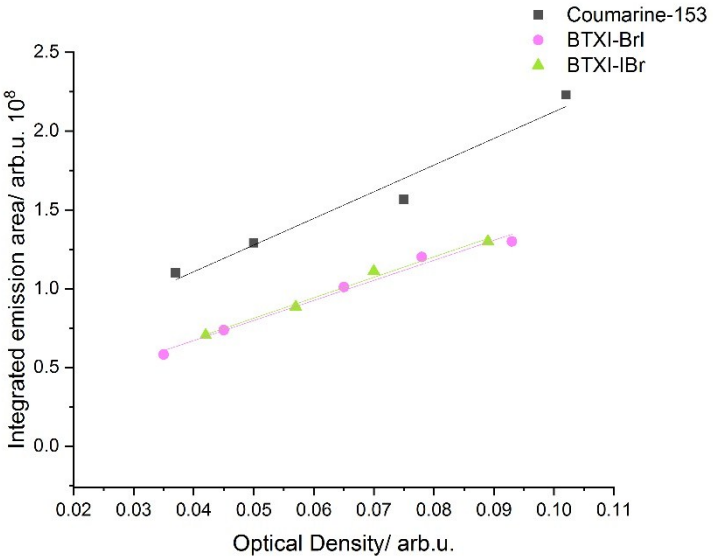

Figure S.15.- Integrated emission area according to optical density of Coumarine-153 (black line) and the BTXI derivatives in DCM at room temperature.

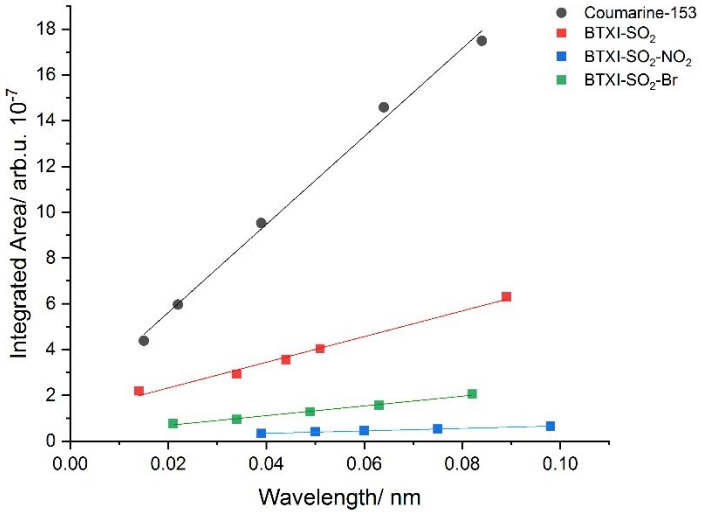

Figure S.16.- Integrated emission area according to optical density of Coumarine-153 (black line) and the $BTXISO_2$ derivatives in DCM at room temperature.

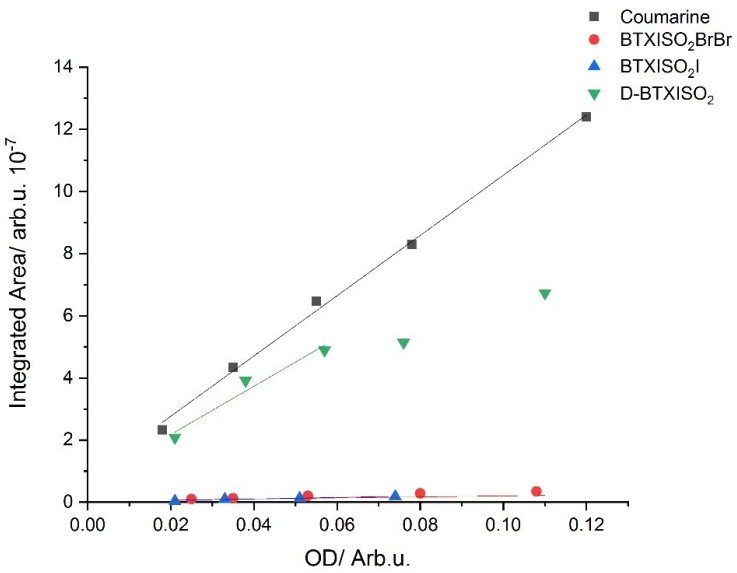

Figure S.17.- Integrated emission area according to optical density of Coumarine-153 (black line) and the $BTXISO_2$ derivatives in DCM at room temperature.

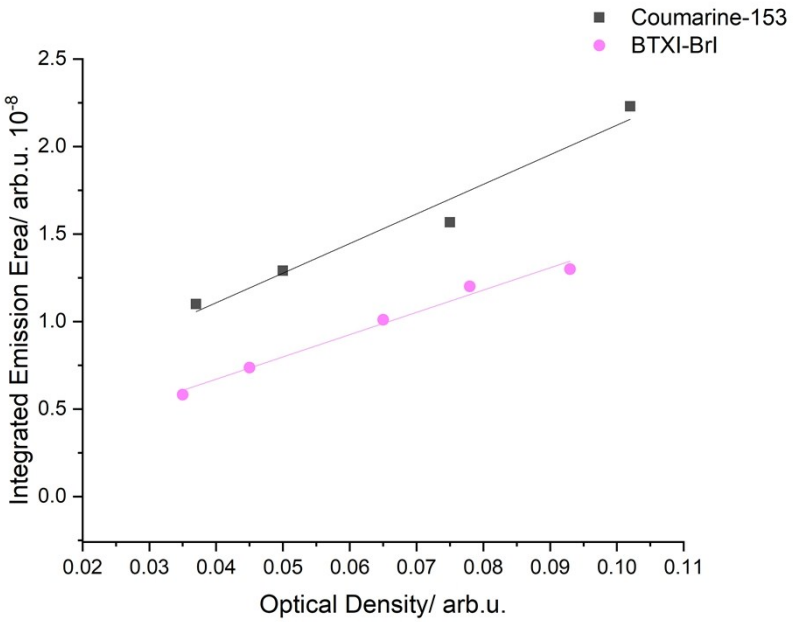

Figure S18.- Integrated emission area according to optical density of Coumarine-153 (black line) and the BTXI-BrI derivative in DCM at room temperature.

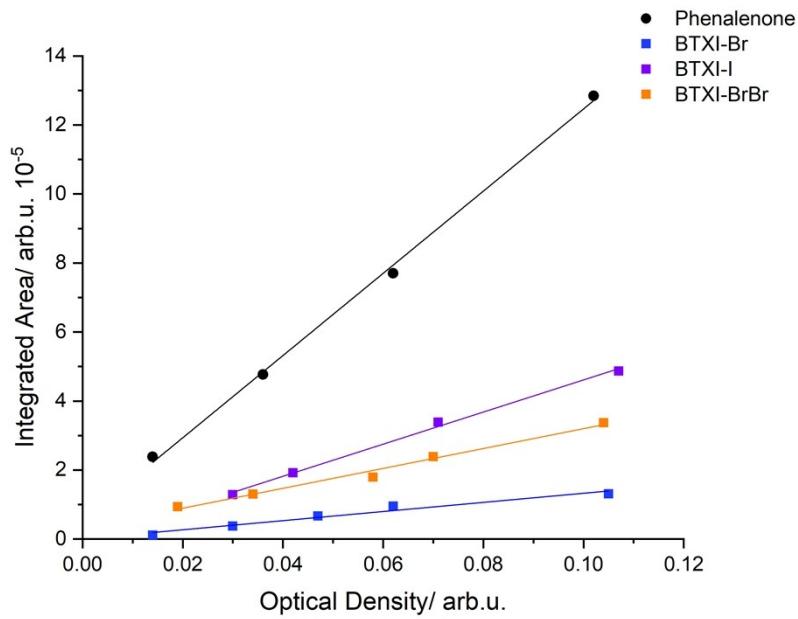

Figure S.19.- Integrated singlet oxygen emission area according to optical density of phenalenone (black line) and the BTXI derivatives in DCM at room temperature.

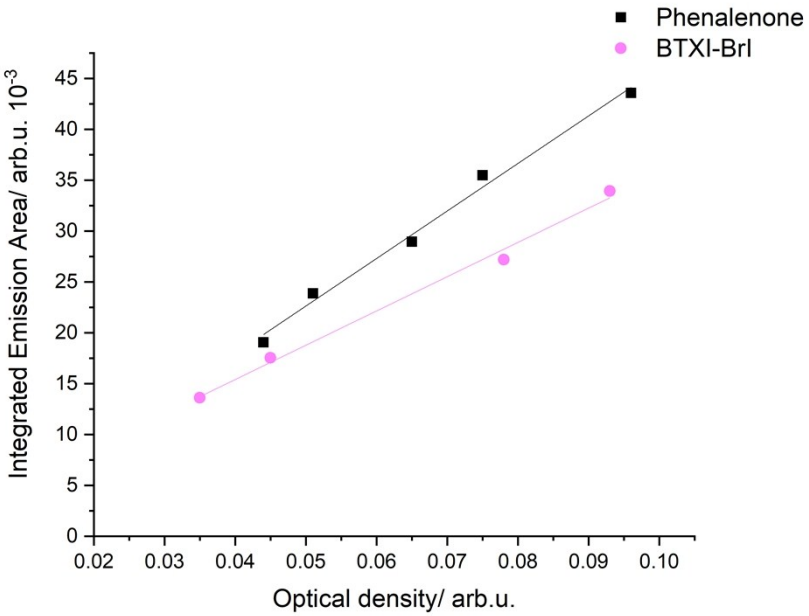

Figure S.20. Integrated singlet oxygen emission area according to optical density of phenalenone (black line) and the BTXI-BrI derivative in DCM at room temperature.

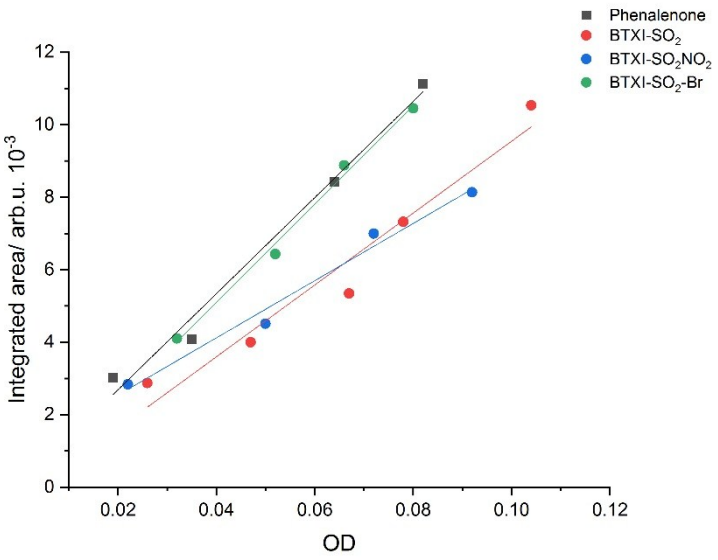

Figure S.21.- Integrated singlet oxygen emission area according to optical density of phenalenone (black line) and the $BTXISO_2$ derivatives in DCM at room temperature.

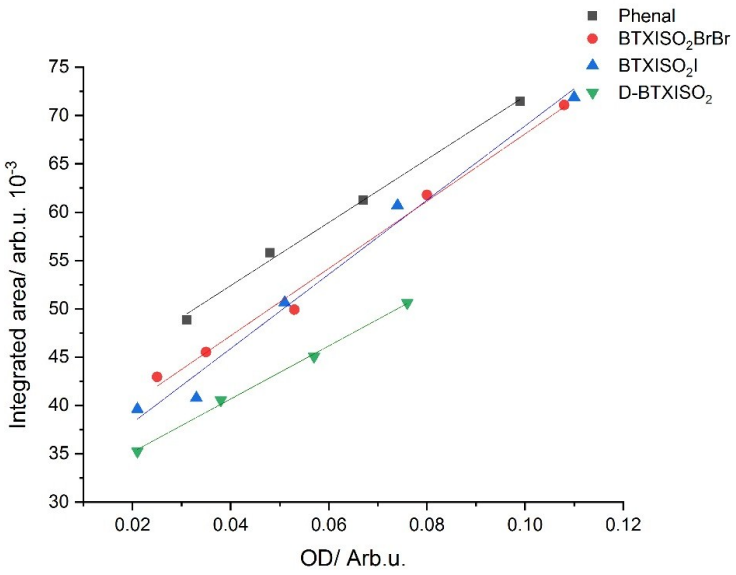

Figure S.22.- Integrated singlet oxygen emission area according to optical density of phenalenone (black line) and the $BTXISO_2$ derivatives in DCM at room temperature.

TD-DFT simulated absorption and fluorescence spectra

The S_0->S_1 transition has almost a purely HOMO->LUMO character. These two orbitals are presented in Figure S_1. For the BTXI-NO_2, the HOMO and LUMO are drawn for both the S_0 stable and S_1 stable geometries to highlight the important change in the nature of the transition upon S_1 relaxation.

<table>
<tr>
<td>BTXI
HOMO LUMO
 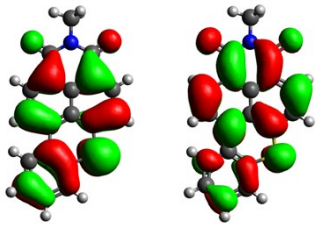 </td>
<td>BTXI-Br
HOMO LUMO
 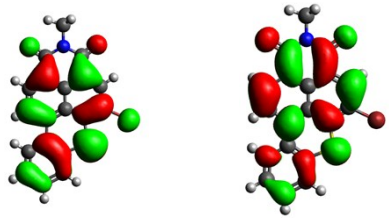 </td>
<td>BTXI-BrBr
HOMO LUMO
 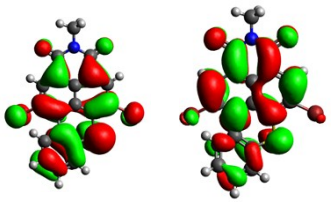 </td>
</tr>
<tr>
<td>BTXI-I
HOMO LUMO
 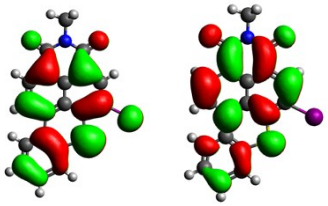 </td>
<td>BTXI-BrI
HOMO LUMO
 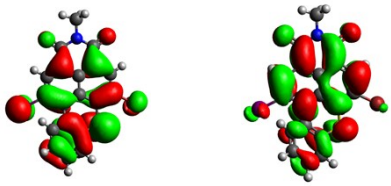 </td>
<td></td>
</tr>
<tr>
<td>BTXI-NO_2
HOMO-S_0geom LUMO-S_0geom
 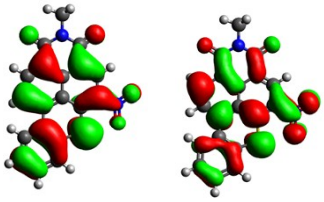
HOMO-S_1geom LUMO-S_1geom
 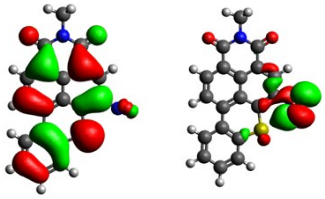 </td>
<td>BTXI-NPh_2
HOMO LUMO
 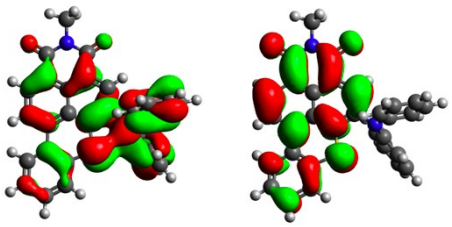 </td>
<td></td>
</tr>
</table>

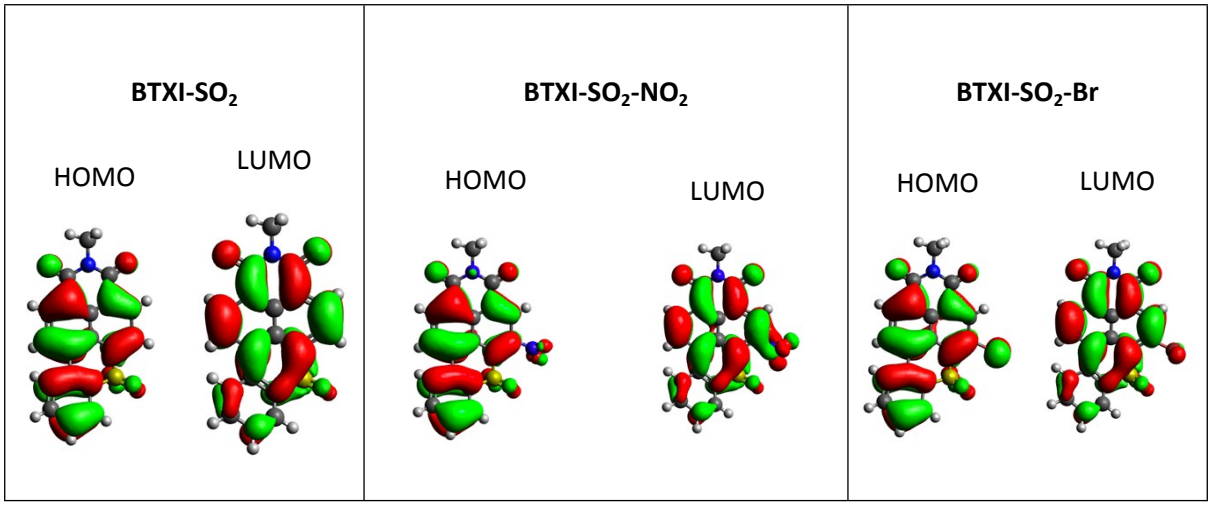

Figure S.23. Computed frontier orbitals (PBE0/PCM/6-311+G(d,p), isovalue 0.02 a.u.)

The absorption spectra of the molecules investigated in this article were simulated by convoluting the TD-DFT transitions with gaussian functions (Figure S2, 0.3 eV of FWHM). The agreement in the shape of the spectra and the positions of the first intense band (in the 400-500 nm region for the BTXI series and in the 350-400 nm region for the BTXI-SO2 series) between theory and experiment is generally very good. In the case of the BTXI-SO2 series, the different shoulders observed on the first experimental band is due to a vibronic coupling, as proven by the simulated vibronically resolved spectra (Figure S3). For the BTXI-NPh2, the inversion of intensity for the two first bands between theory and experiment is probably due several rotation conformers of the NPh_2 group but is not expected to affect the electronic properties of these states.

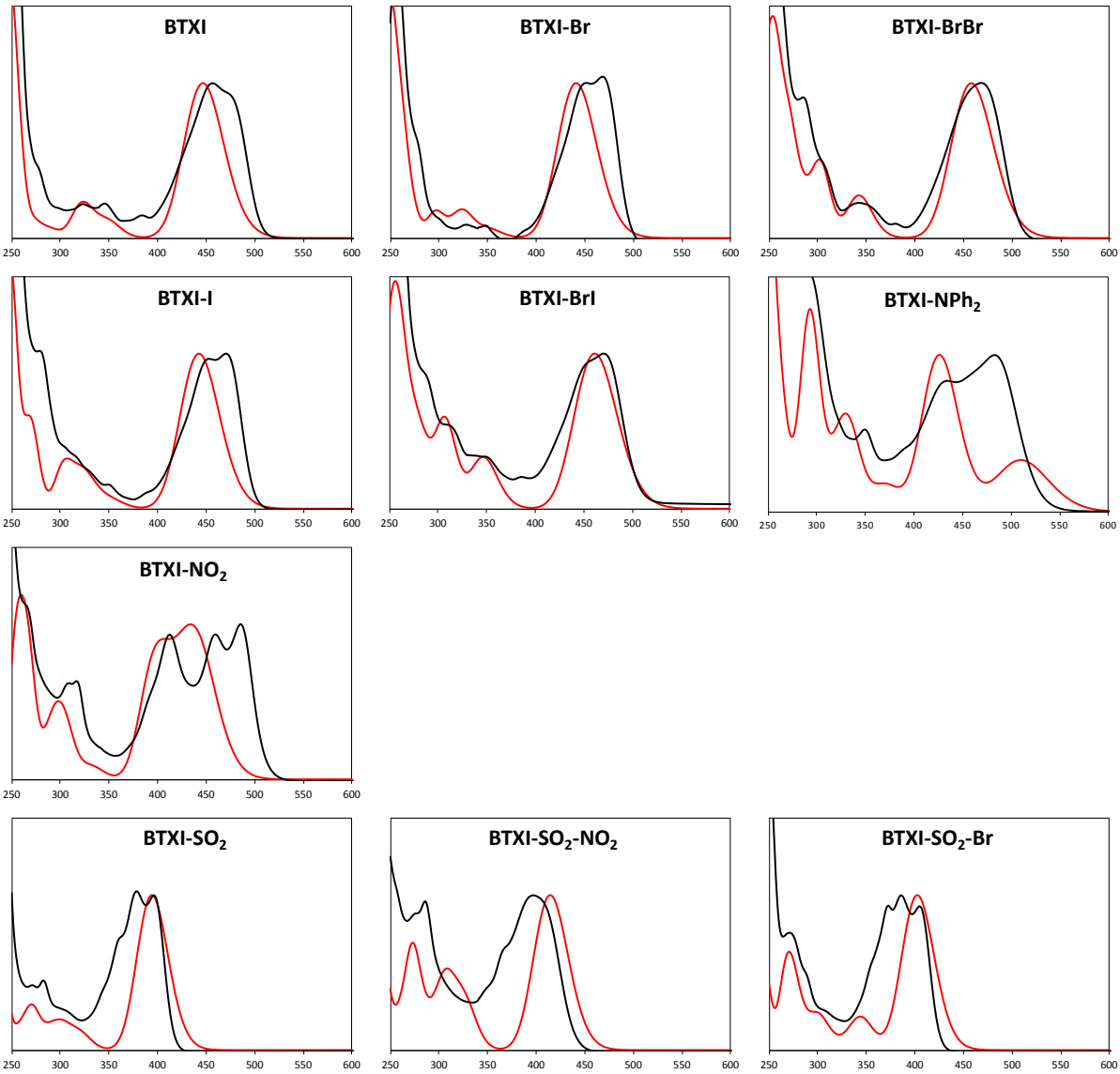

Figure S.24. Simulated (red line) and experimental (black line) absorption in normalized intensity as a function of the incident photon wavelength (in nm).

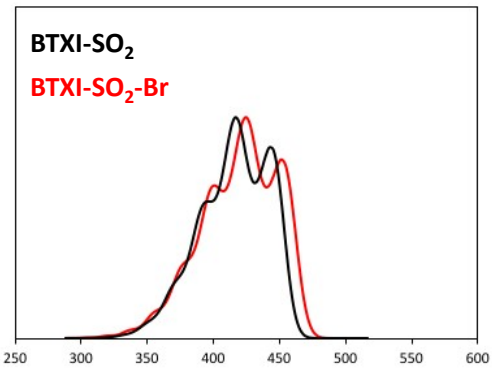

Figure S.25. Simulated vibronically resolved first absorption band of BTXI-SO_2 (black line) and BTXI-SO_2-Br (red line) in normalized intensity as a function of the incident photon wavelength (in nm).

The table S1 presents the measured and computed fluorescence wavelengths. In general, the agreement between theory and experiment is particularly good. The main discrepancy is for the BTXI-NO_2 molecule, but this molecule experiences an important geometry relaxation, characterized experimentally by a large Stokes shift. Computationally, the Stokes shift is over-estimated, but this is probably due to the known tendency of PBE0 functional to underestimate transition energies when the overlap between orbitals associated to a transition is low, as in the case of the HOMO and LUMO of BTXI-NO_2 in the S_1 stable geometry (Figure S1). This is supported by a range-separated hybrid calculation (cam-B3LYP) that partially decrease the discrepancy (table S1).

PBE0 underestimate the transition energies in fluorescence for the BTXI-SO_2 series. Again, this is probably due to the larger charge-transfer character associated to this family of molecules since the distance of charge transfer is computed to be around 3.1 Angtröm for BTXI-SO_2 compared to 2.5 Angtröm for BTXI.

	λ_{em}-RT (exp)	λ_{em} (comp)
BTXI	510	508
BTXI-Br	500	498
BTXI-BrBr	530	540
BTXI-I	505	500
BTXI-BrI	501	547
BTXI-NO_2	585	1006 722 (cam-B3LYP)
BTXI-NPh_2	600	631
BTXI-SO_2	442	482
BTXI-SO_2-NO_2	495	551
BTXI-SO_2-NO_2-Br	455	493

Table S1. Measured and computed fluorescence wavelength.

NMR spectra

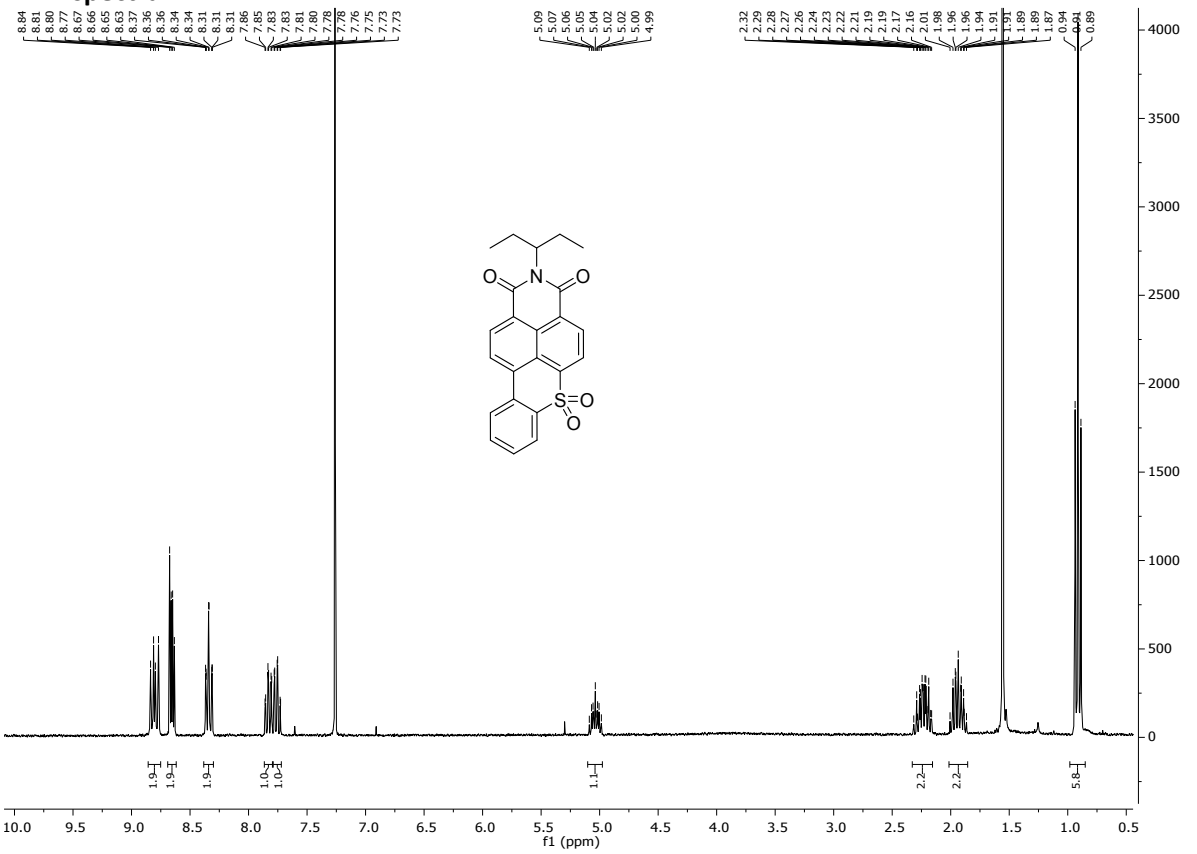

^{1}H NMR ($CDCl_3$, 300 MHz) spectrum of **BTXI-SO_2**.

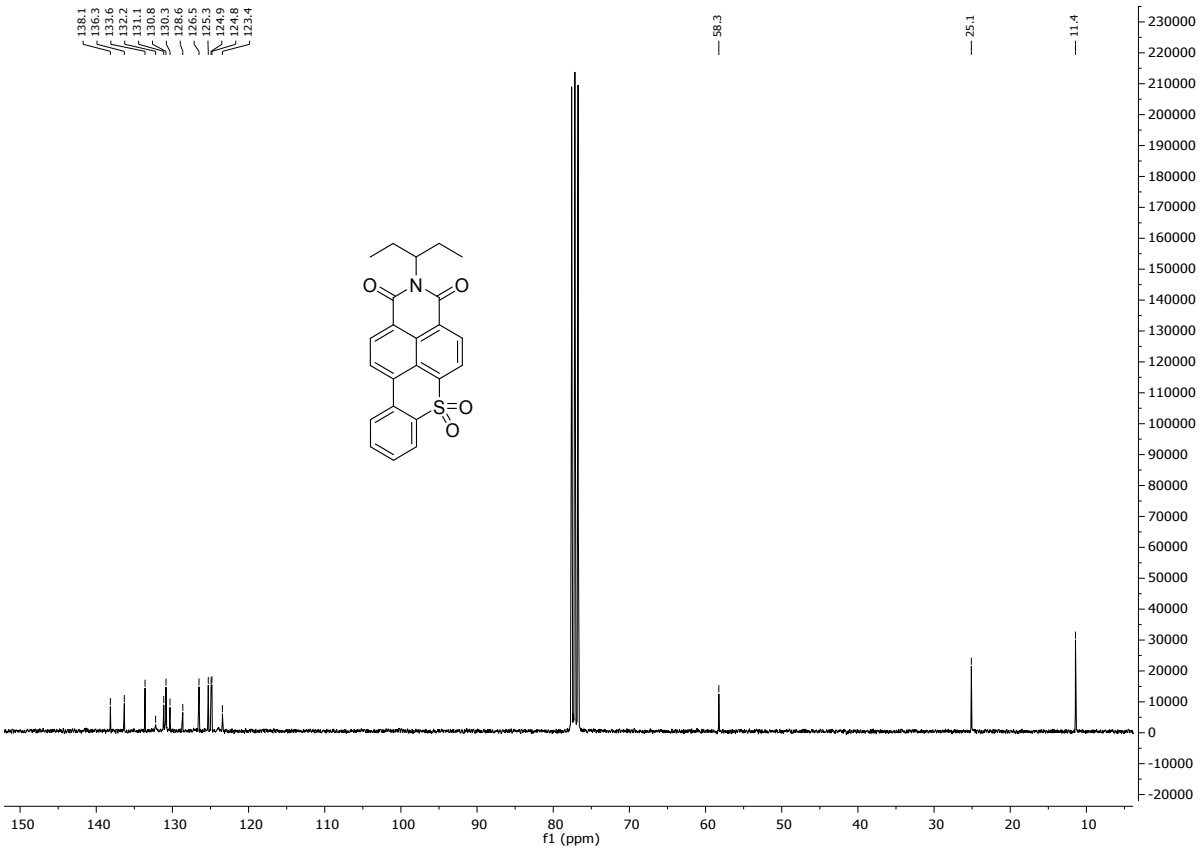

^{13}C NMR ($CDCl_3$, 75 MHz) spectrum of **BTXI-SO_2**.

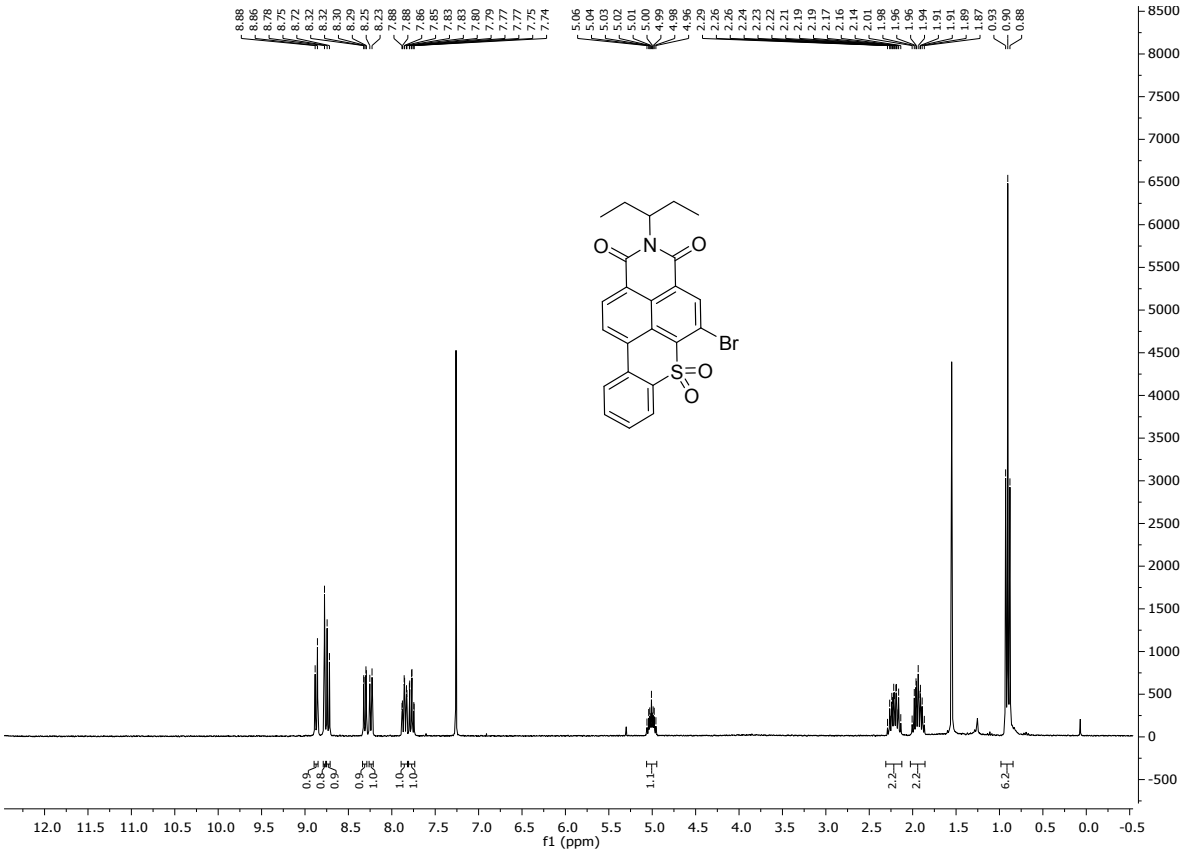

^{1}H NMR ($CDCl_3$, 300 MHz) spectrum of **BTXI-SO_2-Br**.

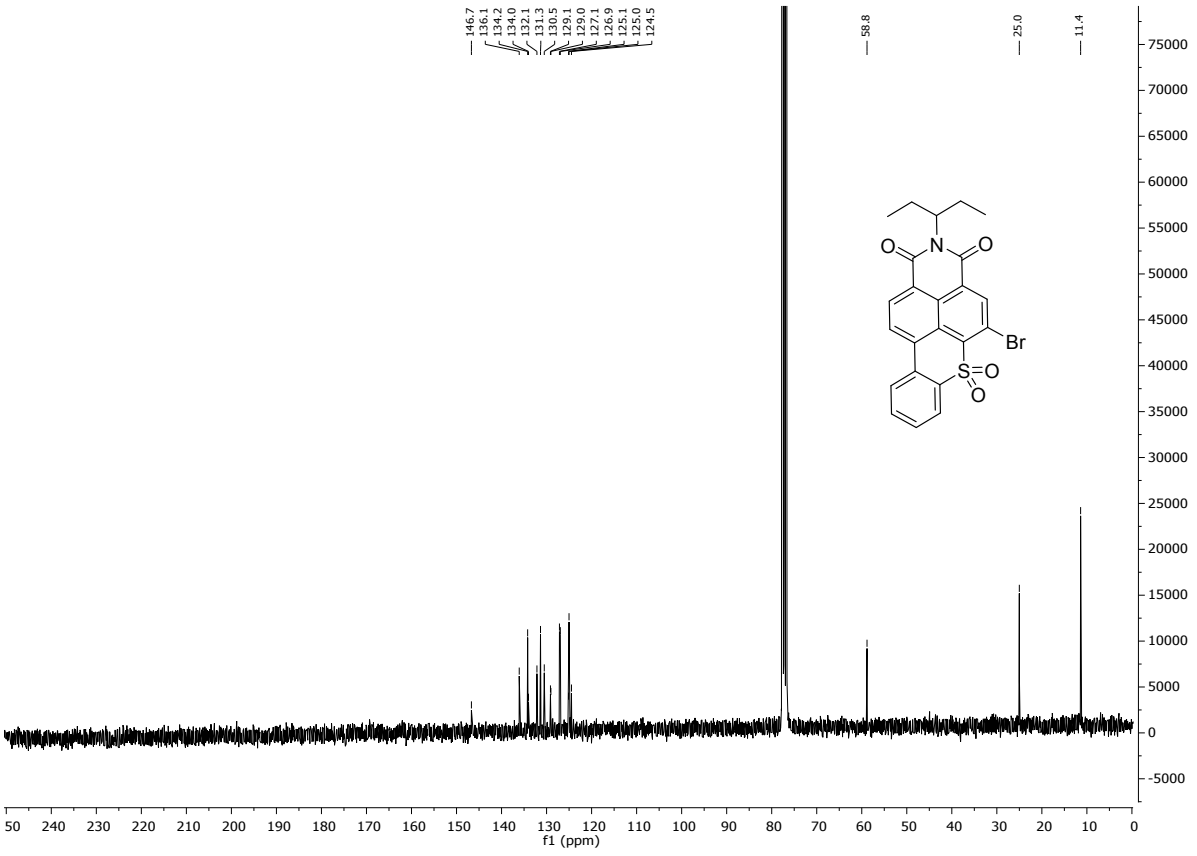

^{13}C NMR ($CDCl_3$, 75 MHz) spectrum of **BTXI-SO_2-Br**.

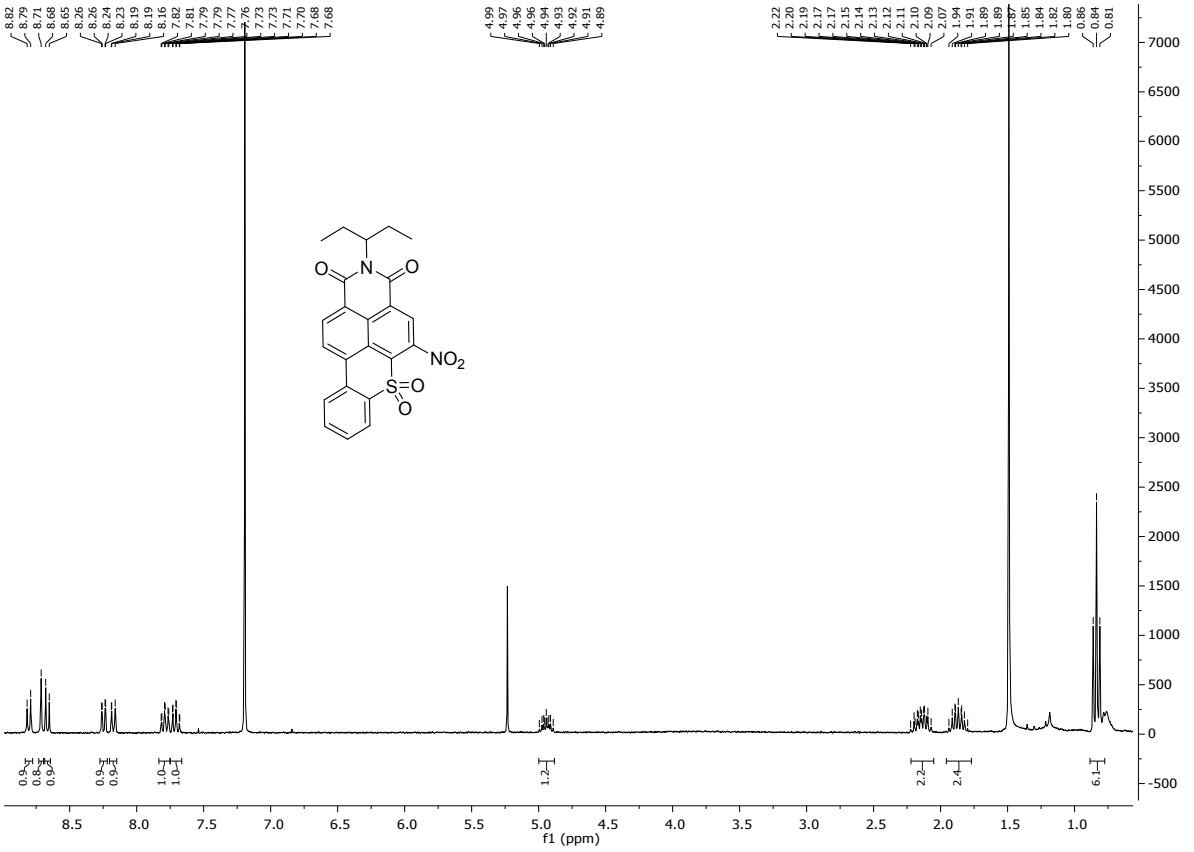

^{1}H NMR ($CDCl_3$, 300 MHz) spectrum of **BTXI-SO_2-NO_2**.

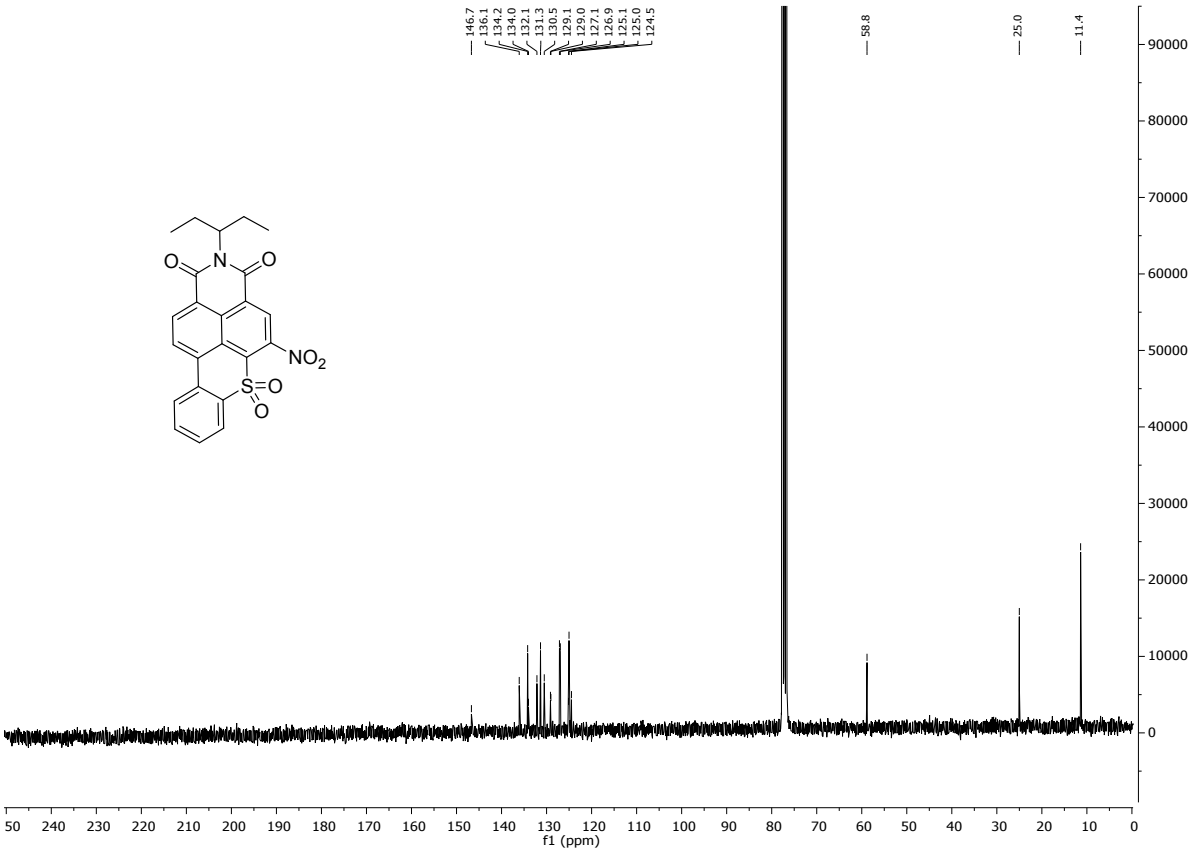

^{13}C NMR ($CDCl_3$, 75 MHz) spectrum of **BTXI-SO_2-NO_2**.

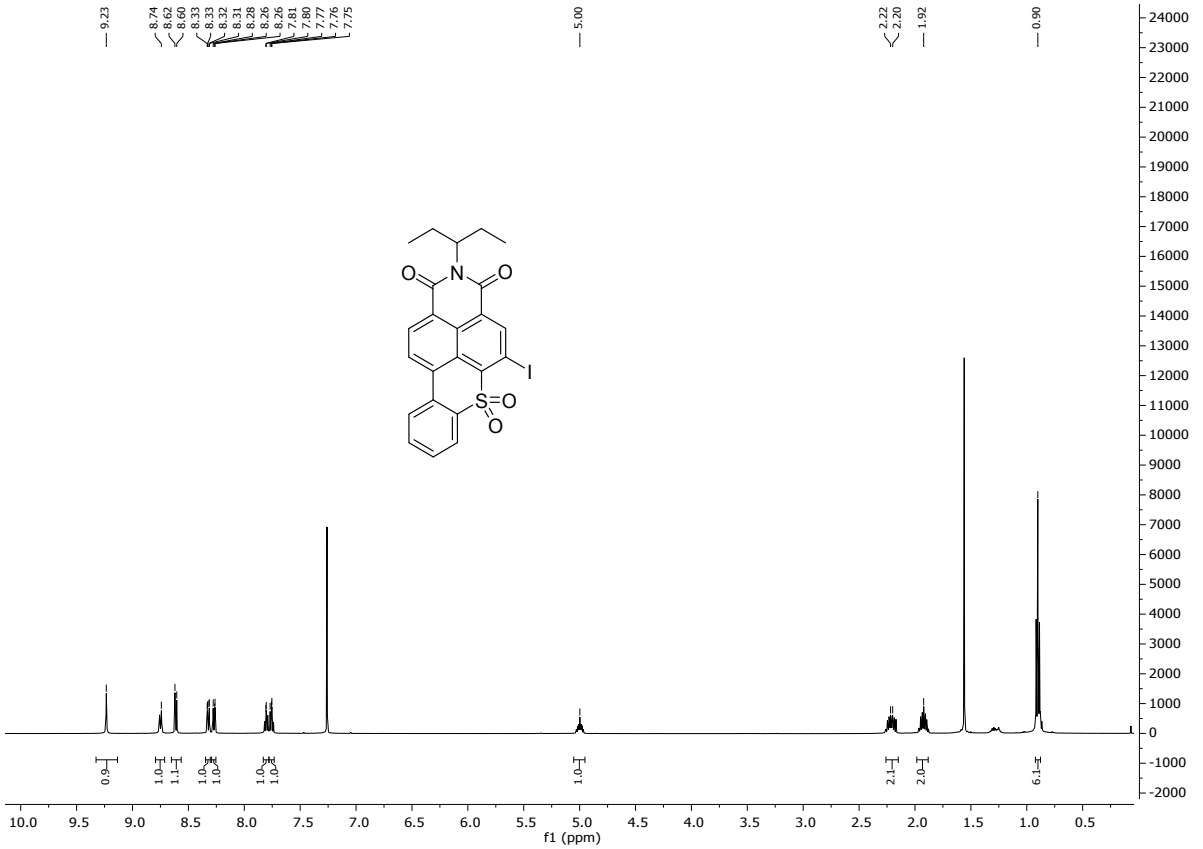

^{1}H NMR ($CDCl_3$, 500 MHz) spectrum of **BTXI-SO_2-I**.

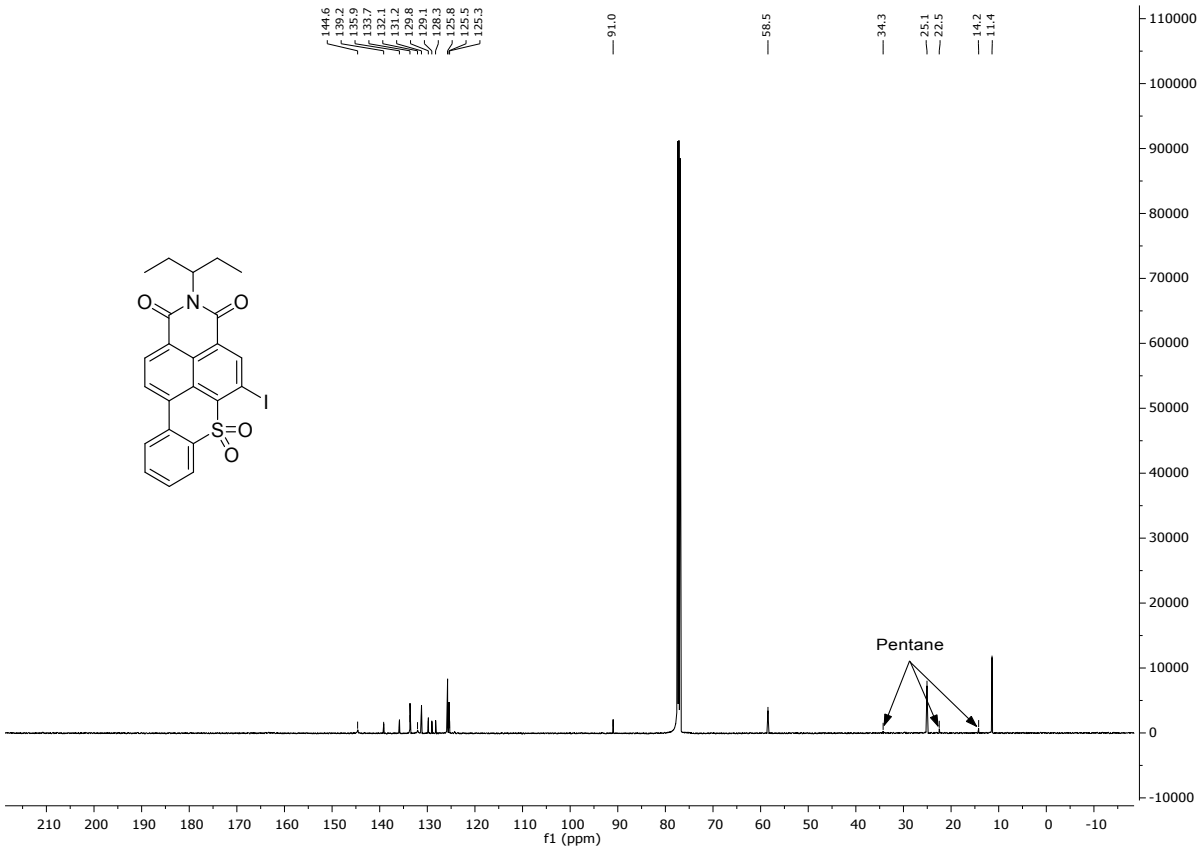

^{13}C NMR ($CDCl_3$, 125 MHz) spectrum of **BTXI-SO_2-I**.

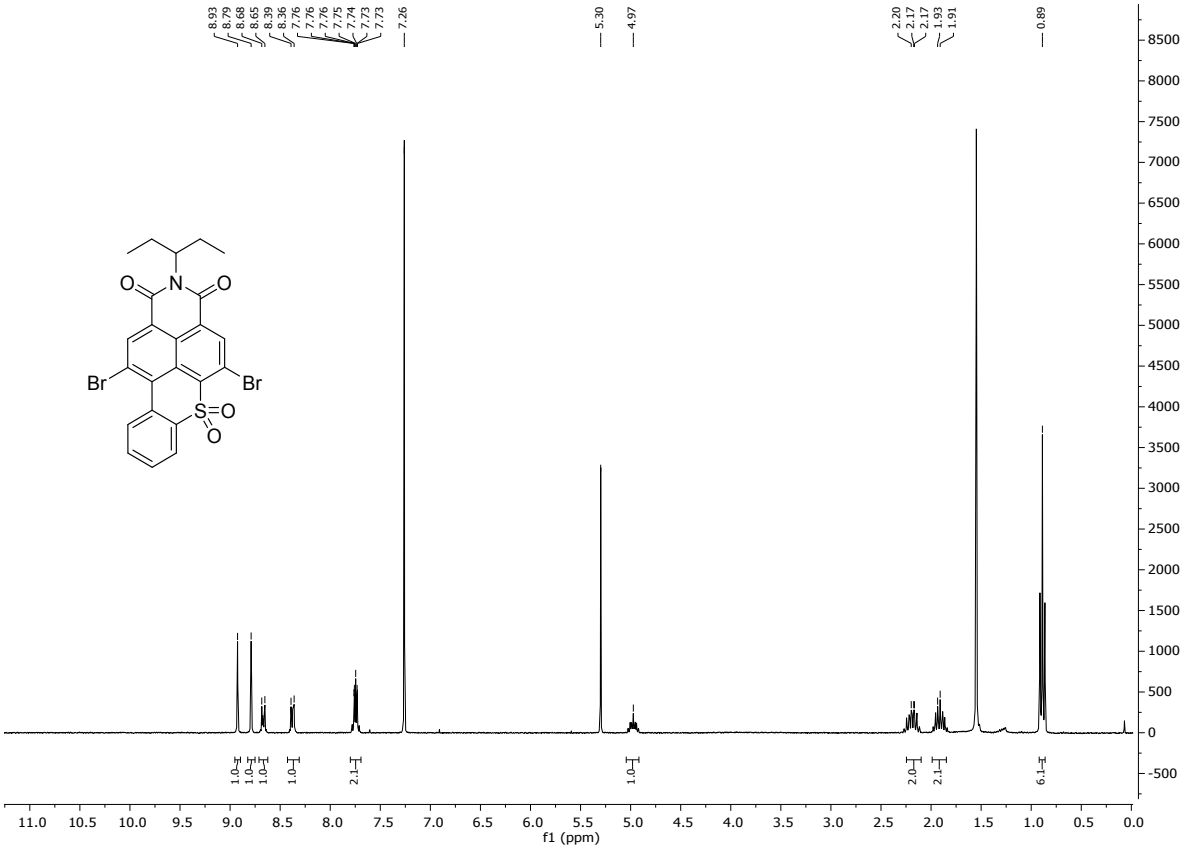

^{1}H NMR ($CDCl_3$, 300 MHz) spectrum of **BTXI-SO_2-Br**.

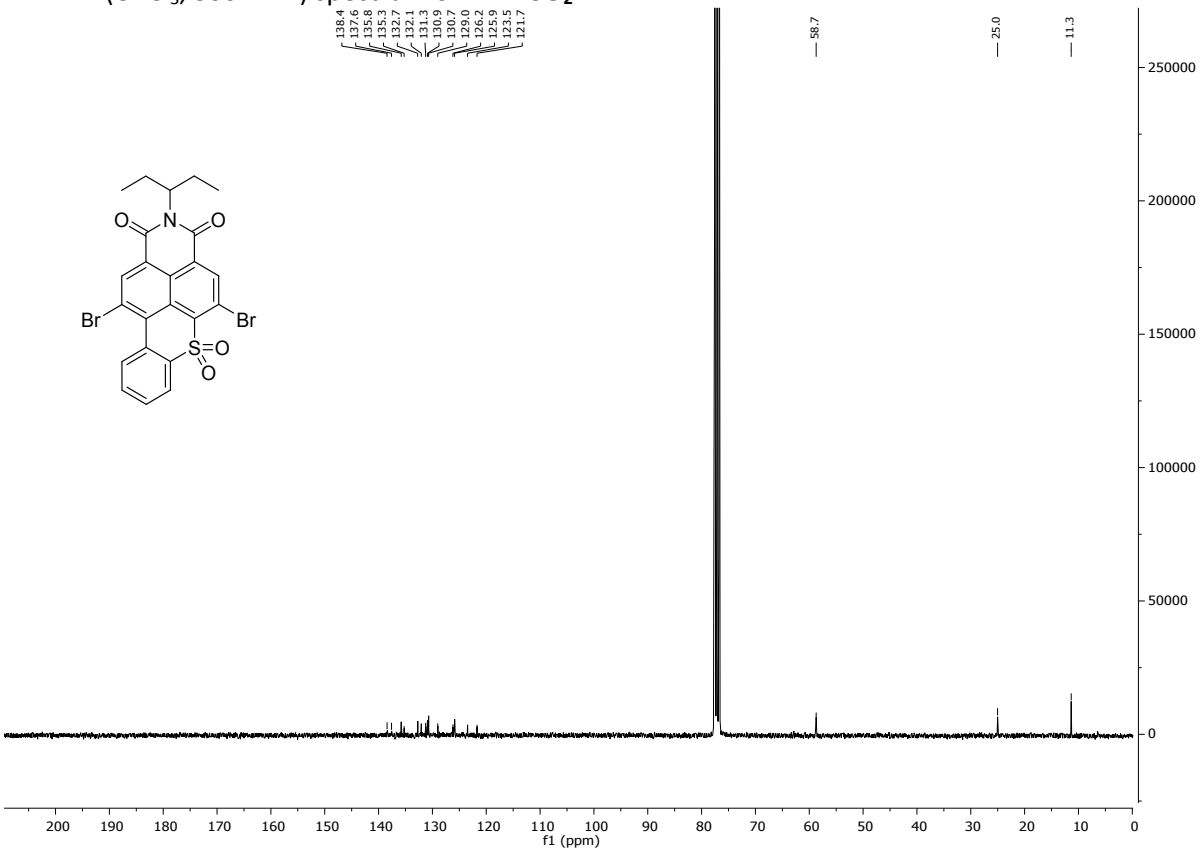

^{13}C NMR ($CDCl_3$, 75 MHz) spectrum of **BTXI-SO_2-BrBr**.

Mass Spectra

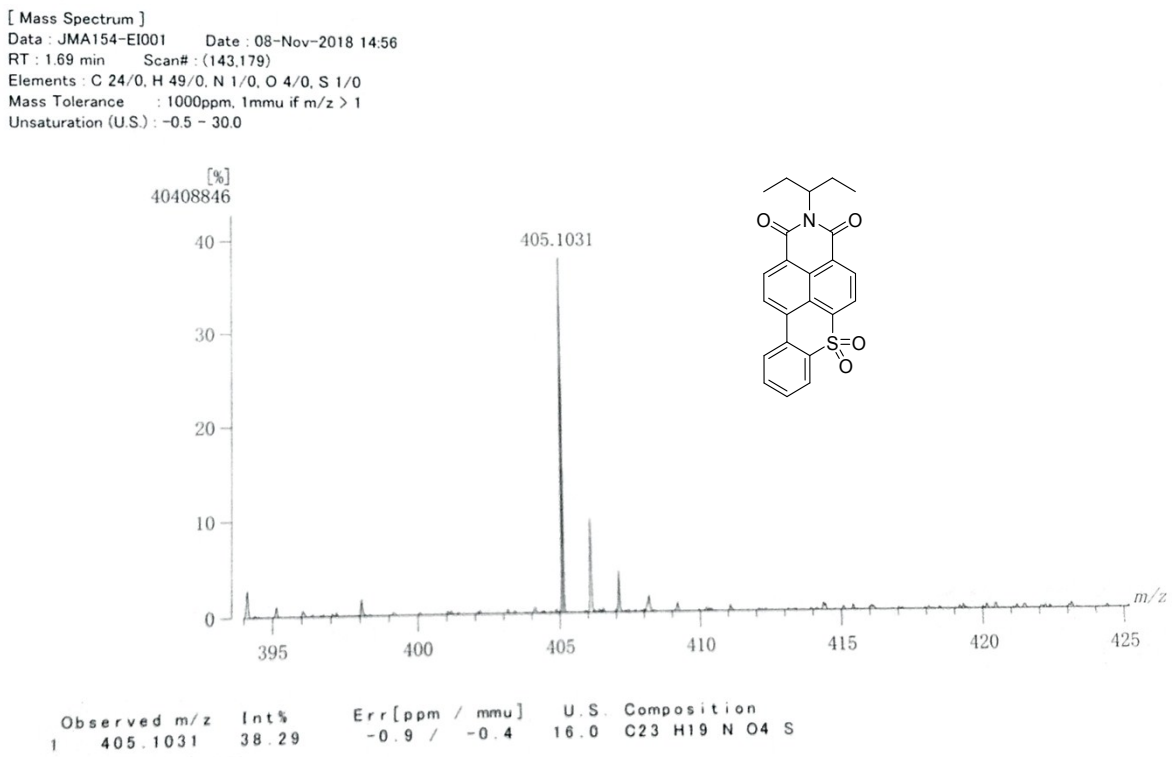

HRMS (EI) of **BTXI-SO_2**: *m/z* calcd for $C_{23}H_{19}NO_4S$: 405.1029, found: 405.1031.

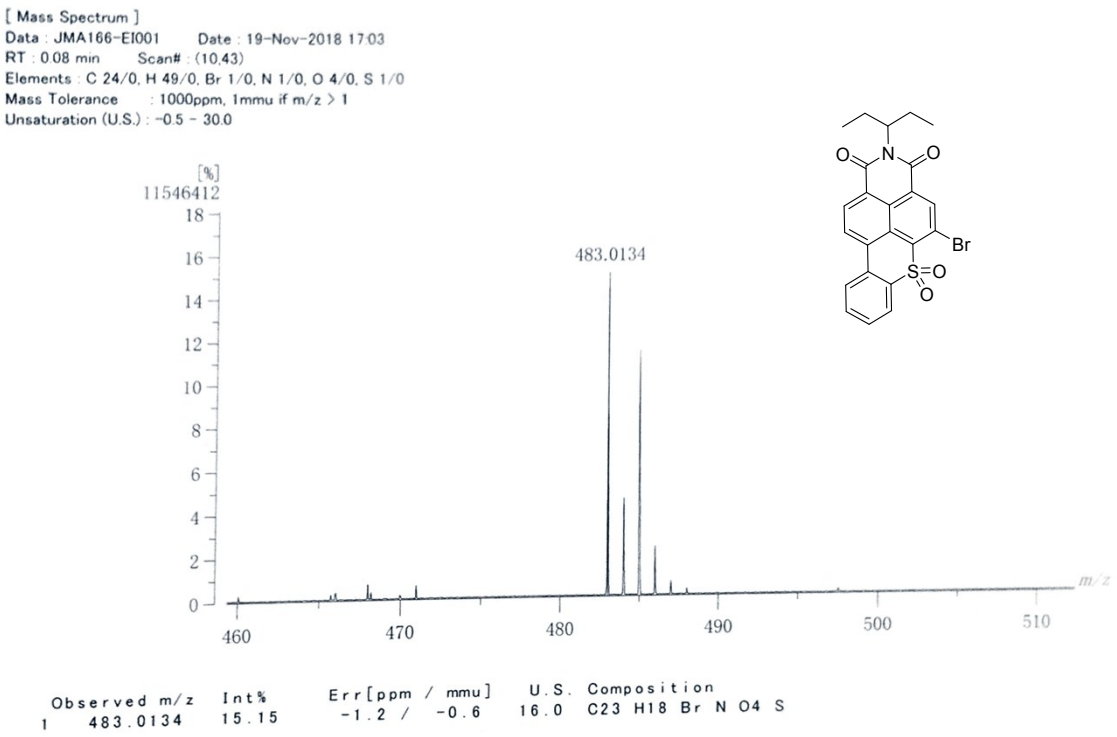

HRMS (EI) of **BTXI-SO_2-Br**: *m/z* calcd for $C_{23}H_{18}BrNO_4S$: 483.0134, found: 483.0134.

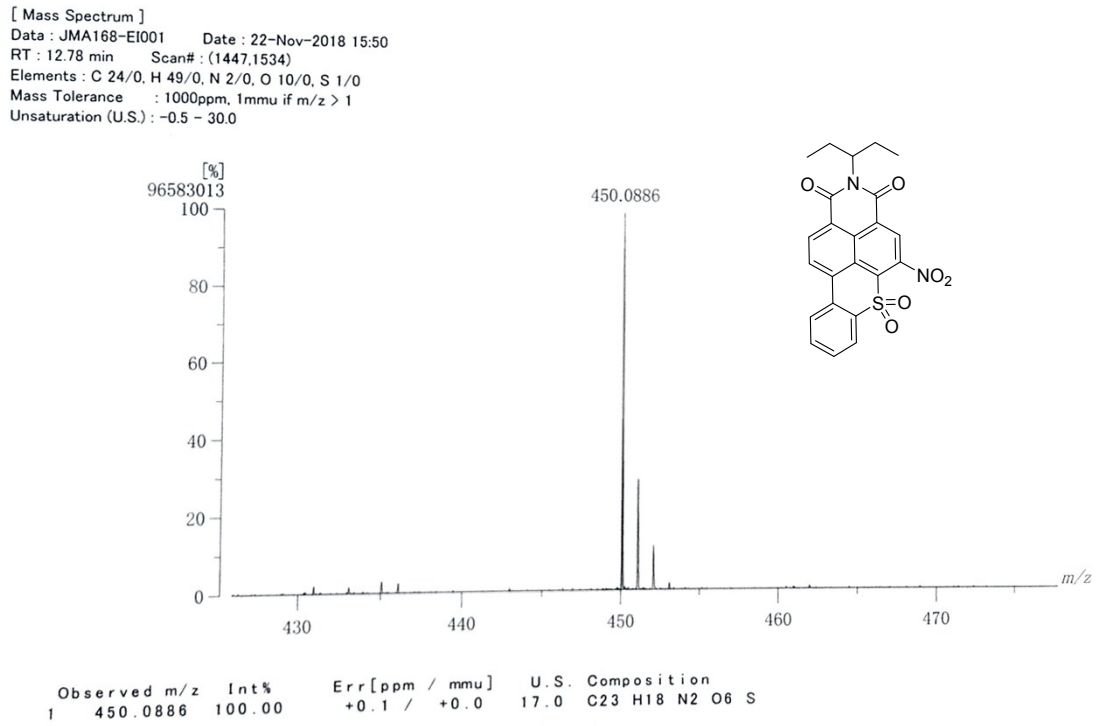

HRMS (EI) of **BTXI-SO_2-NO_2**: *m/z* calcd for $C_{23}H_{18}N_2O_6S$: 450.0880, found: 450.0886.

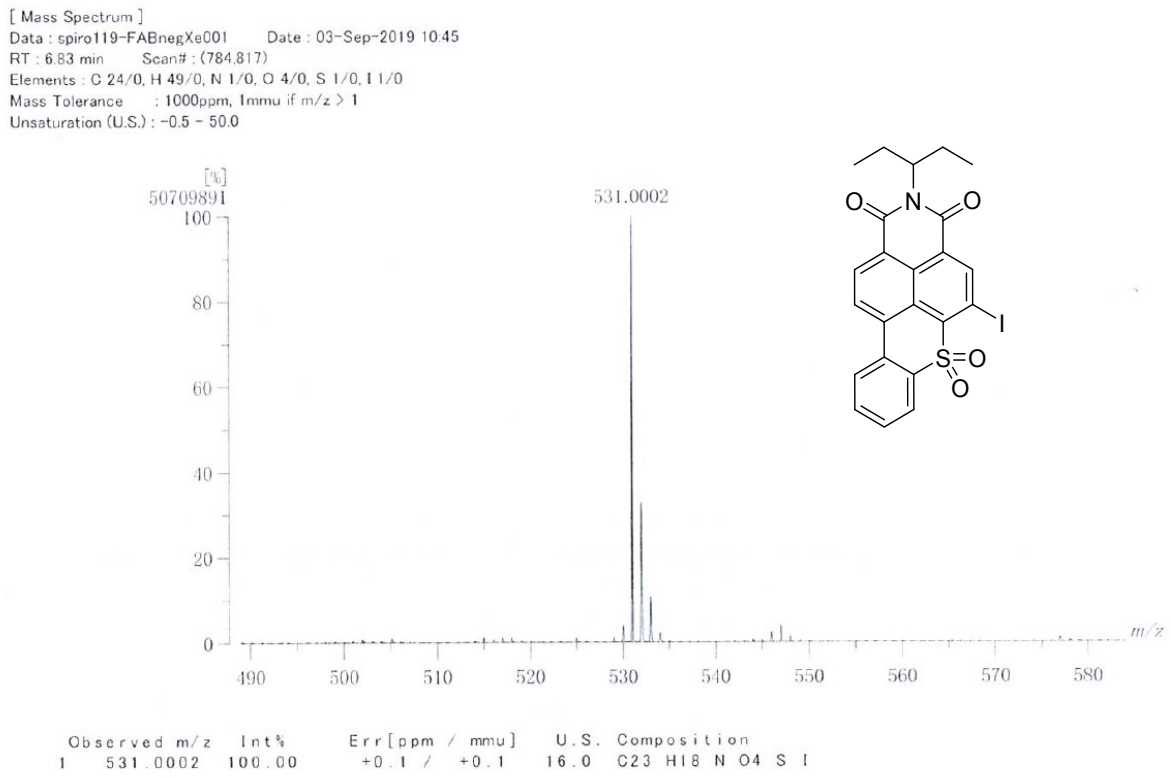

HRMS (FAB-neg) of **BTXI-SO_2-I**: calcd for $C_{23}H_{18}INO_4S$: 531.0001, found: 531.0002.

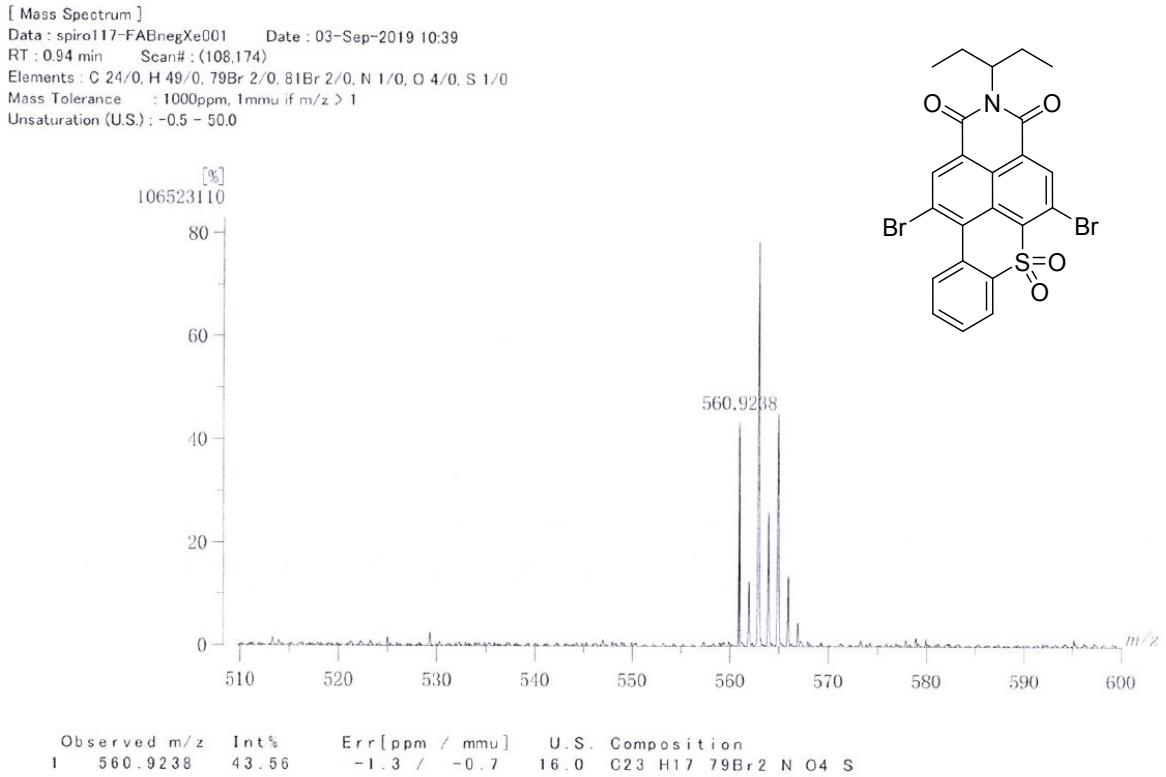

HRMS (FAB-neg) of **BTXI-SO_2-BrBr**: calcd for $C_{23}H_{17}Br_2NO_4S$: 560.9245, found: 560.9238.